







# Peroxide-based crosslinking of solid silicone rubber, part II: The counter-intuitive influence of dicumylperoxide concentration on crosslink effectiveness and related network structure

M. Azevedo<sup>1</sup>  | A.-M. Monks<sup>1</sup> | R. C. Kerschbaumer<sup>1</sup>  | S. Schlögl<sup>1</sup>  |  
K. Saalwächter<sup>2</sup>  | M. Walluch<sup>3</sup> | G. Consolati<sup>4</sup>  | C. Holzer<sup>5</sup> 

<sup>1</sup>Polymer Competence Center Leoben GmbH, Leoben, Austria

<sup>2</sup>Institut für Physik – NMR, Martin-Luther Universitaet Halle-Wittenberg, Halle (Saale), Germany

<sup>3</sup>Anton Paar GmbH, Graz, Austria

<sup>4</sup>Department of Aerospace Science and Technology, Politecnico di Milano, Milan, Italy

<sup>5</sup>Department of Polymer Engineering and Science, Polymer Processing, Montanuniversitaet Leoben, Leoben, Austria

## Correspondence

C. Holzer, Department of Polymer Engineering and Science, Polymer Processing, Montanuniversitaet Leoben, Franz-Josef Strasse 18, 8700 Leoben, Austria.

Email: [clemens.holzer@unileoben.ac.at](mailto:clemens.holzer@unileoben.ac.at)

## Funding information

Österreichische Forschungsförderungsgesellschaft, Grant/Award Number: 879785

## Abstract

Application of elastomers in general demands the conversion of their soluble networks into crosslinked structures. This abrupt change causes several modifications, both in the atomic/molecular level and at the macro-scale. In this study, solid silicone rubber (high molecular weight poly(dimethylsiloxane)), was crosslinked with dicumylperoxide (DCP), a widely used crosslinking agent by the rubber industry. The changes caused by different DCP concentrations were investigated, aiming to bring attention to the molecular transformations, usually neglected when processing-oriented studies are conducted. DCP concentration showed a limited contribution to the network's molecular dynamics, which was found to be mainly dominated by entanglements. The dominance of entanglements over other molecular constraints, like crosslink points, justifies the threshold and counter-intuitive behavior of tensile and hardness properties. However, differences were found in the crystallization ability after crosslinking, when the more crosslink points were introduced, the lower the crystallinity was and the less stable the PDMS crystallites were. In addition to providing a deeper understanding of an industrially applied rubber system *n* terms of the effective concentration of DCP, and the reasoning behind such concentration, the findings of this study add to the state-of-the-art comprehension of elastomeric networks, and how they behave on a molecular level.

## KEYWORDS

crosslink density, crosslinking, dicumylperoxide, free volume, network morphology, silicone

## 1 | INTRODUCTION

Poly(siloxane)s of high molecular weight, known as silicone elastomers or silicone rubbers, are materials

composed of hybrid macromolecules: the main chain is based on successive silicon-oxygen bonds (inorganic), and the side groups (attached to the tetravalent Si-atom) are monovalent organic moieties, such as methyl or

This is an open access article under the terms of the [Creative Commons Attribution](https://creativecommons.org/licenses/by/4.0/) License, which permits use, distribution and reproduction in any medium, provided the original work is properly cited.

© 2023 The Authors. *Journal of Applied Polymer Science* published by Wiley Periodicals LLC.

phenyl. This alternating inorganic chain of Si and O atoms grants unique properties to silicone, like strong and long chain bonds,<sup>1</sup> main chain flexibility,<sup>2</sup> low inter- and intramolecular forces, and good dielectric properties.<sup>3,4</sup> As a result of the longer Si—O bond, compared to a C—C bond, there is more space for organic side groups, like methyl and phenyl, without an increase in steric hindrance or molecular congestion, thus retaining flexibility. The flexibility of the Si—O—Si bond is explained by the oxygen atom's delocalized lone electron pair, which is spread over the covalent bond region between Si and O atoms, specifically into the silicon vacant d orbital, allowing a wider angle for the sp<sup>3</sup> hybridization. These molecular properties, linked to the inorganic nature of the main chain and the organic nature of the side group substituent, constitute an important bridge between inorganic and well-known organic polymers. Nowadays, silicone rubber has been used to produce medical devices, optical components, sealants, and electronic parts, for example.<sup>2,5–7</sup>

In spite of the high molecular weight, silicone rubber must be crosslinked in order to be employed to manufacture usable products. The curing reaction shifts the soluble and highly viscous state of the polymer into an insoluble and viscoelastic condition. It was already reported by this group,<sup>8</sup> and also widely cited in the literature,<sup>9–11</sup> that a dicumylperoxide (DCP)-based silicone rubber crosslinking mechanism involves free radicals, which act in accordance with kinetic and thermodynamic boundaries. These free radicals are able to abstract protons from the silicone chain (specifically at the organic side groups), creating active sites for crosslinking. Ultimately, what was only an entangled silicone network becomes a tridimensional network, where entanglements and chain junctions co-exist. All properties that characterize the final crosslinked silicone product are derived from this tridimensional network, being mainly dependent on the density of chain junctions, or crosslink density. Thus, this study aims to present a comprehensive characterization of industrially relevant DCP-cured compounds regarding the effect of the crosslinking reaction in macro- and micro properties. It is based upon our previous study<sup>8</sup> on the crosslinking mechanism of the same silicone compounds in terms of kinetic and thermodynamic considerations. This combination of kinetic, thermodynamic, and now molecular dynamic-based investigation of an industrially significant material contributes not only to the understanding of peroxide-cured poly(siloxane)s, but also to polymeric systems with similar chemistry and molecular structure, such as organic elastomers. Besides, the correlation among molecular characteristics and bulk properties is novel for peroxide-crosslinked

silicones, explaining the usual concentration of DCP applied in the industry (up to 1 phr), and the behavior described in the literature, such as the studies of Kruželák et al.<sup>12</sup> and Verheyen et al.<sup>13</sup> but not yet elucidated.

## 2 | MATERIALS AND METHODS

This section describes all characterization techniques and the necessary knowledge to calculate and interpret their results. State-of-the-art definitions related to the following methods were suppressed when not essential for understanding the reported results.

### 2.1 | Materials

High consistency poly(dimethylsiloxane), or solid PDMS (Xiameter™ RBB-2100-50,  $M_w = 660 \text{ kg mol}^{-1}$ ,  $M_w/M_n = 1.8$ ), containing approximately 26 wt% of an inorganic filler and no significant concentration of vinyl side groups (as confirmed by <sup>1</sup>H-NMR studies) was supplied by Dow Inc. (Midland, MI, USA). PDMS characterization in terms of molecular weight, filler, and vinyl contents is described in a previous publication of the present research group.<sup>8</sup> DCP 99.9% (Peroxan DC, Pergan GmbH, Bocholt, Germany) was supplied with an active oxygen content of 5.91 wt%. Both components were thoroughly mixed in a 2-roll-mill by Biesterfeld Interowa GmbH & Co (Vienna, Austria) varying the peroxide concentration: 0, 0.21, 0.35, 0.49, 0.70, 1.00, and 1.50 phr of DCP. These concentrations represent fractions of the suggested peroxide concentration (0.70 phr) by the silicone supplier, that is, 0%, 30%, 50%, 70%, 100%, 140%, and 215%. The samples up to 0.70 phr were prepared at the same time, employing the same PDMS and DCP batches, while the samples with higher DCP concentrations were produced afterwards. Differences between these two groups may arise due to batch variations, such as molecular weight distribution, or  $M_w$ . These variations are assigned whenever they are present, but these do not compromise the comparability between the studied samples. All silicone compounds were stored at low temperatures (<5°C) prior to testing, in order to avoid pre-curing.

### 2.2 | Preparation of cured PDMS plates

Crosslinking of the PDMS/DCP compounds into cured plates was conducted in a vertical hot molding press (MTF750 160editionS MAPLAN GmbH, Kottlingbrunn,

Austria) via compression molding. The curing cycle had a duration of 20 min at 160°C for all compounds, regardless of the peroxide content, producing 2 and 6 mm thick plates. In order to guarantee that all DCP was consumed within the compression molding cycle disregarding the DCP concentration, and that all samples had the same thermal history, the same cycle time (longer than the optimum cure time as determined by the rubber process analyzer<sup>8</sup>) was used for all compounds. For peroxide-cured rubber compounds, reversion effects (decrease of the mechanical properties after long curing times) can be neglected, so the curing time for the present study was higher than the optimum cure determined by the rubber process analyzer.<sup>8</sup> Mold temperature was chosen as the one usually applied for processing PDMS via compression molding, with decent curing times and according to the manufacturer. Subsequently, after mold opening, the cured plates were submerged in cold water (5°C) for 10 min, aiming to cease the crosslinking reaction.

### 2.3 | Dynamic scanning calorimetry

Detection of thermal events, such as crystallization, melting, and crosslinking of the DCP/PDMS compounds was carried out using a dynamic scanning calorimeter (DSC1 STAR System Mettler-Toledo International Inc, Greifensee, Switzerland). Non-crosslinked samples (triplicate) were placed into aluminium crucibles, following a specific procedure to guarantee maximum sample contact with the DSC crucible. To do so, the samples were cold-pressed (room temperature) into 2 mm plates, from which disks were punched out. These disks were subsequently introduced into the DSC crucible and pressed against the crucible's bottom. Finally, the samples were submitted to the following thermal program, under 50 mL.min<sup>-1</sup> of nitrogen as purge gas, in random order to avoid any unmeasured, and uncontrolled, disturbances from the laboratory environment and from the device:

1. Isotherm for 5 min at 25°C.
2. Cooling at -10 K min<sup>-1</sup> until -80°C.
3. Isotherm for 10 min at -80°C.
4. Heating at 10 K min<sup>-1</sup> until 220°C.
5. Isotherm for 5 min at 220°C.
6. Cooling at -10 K min<sup>-1</sup> until -80°C.
7. Isotherm for 10 min at -80°C.
8. Heating at 10 K min<sup>-1</sup> until 220°C.

During steps 1, 2, 3, and 4, the sample is considered as non-crosslinked, since the crosslinking reaction is

promoted by the temperature increase only at step 4. The isotherms at -80°C (steps 3 and 7) were set to guarantee full crystallization of the samples. Similarly, the isotherm at 220°C (step 5) was set to ensure the total consumption of DCP for crosslinking promotion. At steps 6, 7, and 8 the samples are considered as fully crosslinked. Step 1 was set to guarantee that all thermal programs start at the same temperature.

The endothermic event related to PDMS crystallites' melting was analyzed during heating and compared for non-crosslinked (step 4) and crosslinked (step 8) samples, in terms of melting enthalpy and heat flow apex temperature. Alike, the exothermic event related to the DCP-driven crosslinking reaction (step 4) was analyzed in terms of the curing enthalpy, calculated after considering baseline correction (step 8) of the heat flow  $\dot{Q}$ . As advised by Heinze and Echtermeyer,<sup>14</sup> the melting ( $H_m$ ) and crosslinking ( $H_x$ ) enthalpies were calculated (mean value) as follows, considering the heating rate  $\beta = 10 \text{ K}\cdot\text{min}^{-1}$ :

$$H_{m,x}, J g^{-1} = \frac{1}{\beta} \int_{T_{\text{onset}}}^{T_{\text{endset}}} \dot{Q} dT. \quad (1)$$

### 2.4 | Equilibrium solvent swelling

Equilibrium swelling experiments were performed at 23°C employing an analytical scale and using toluene (molar volume  $V_{m,\text{toluene}} = 106.2 \text{ mL mol}^{-1}$ , density  $\rho_{\text{toluene}} = 0.86 \text{ g cm}^{-3}$ ) as the solvent. For each DCP concentration, three specimens (triplicate, disk-shaped, 6 mm thick and 10 mm diameter) were weighed (the initial mass was taken as  $m_{\text{initial}}$ ) and then placed inside glass vials with toluene, protected from light. After 48 h, the swollen samples were slightly blotted with tissue paper and immediately weighed (the swollen mass was taken as  $m_{\text{swollen}}$ ). To determine the dry mass after swelling (taken as  $m_{\text{dry}}$ ), the samples were dried for 24 h under forced air circulation and subsequently for 24 h at 50°C in an oven until constant weight was reached. All steps related to the swelling experiments were performed identically, without variations, and all samples were investigated at the same time, utilizing the same solvent batch, and under the same laboratory conditions. The same *modus operandi* for all samples is important, due to the intrinsic high error<sup>15</sup> associated with this method. A more detailed description of the swelling experiment is disclosed at the end of this subsection.

The swelling degree (SD, %) and the toluene-soluble fraction ( $\text{Sol}_{\text{tol}}$ , %) were calculated according to Equations (2) and (3), respectively.

$$\text{SD, \%} = \frac{m_{\text{swollen}} - m_{\text{dry}}}{m_{\text{dry}}} 100, \quad (2)$$

$$\text{Sol}_{\text{tol}}, \% = \frac{m_{\text{initial}} - m_{\text{dry}}}{m_{\text{initial}}} 100. \quad (3)$$

In order to calculate the crosslink density, the thermodynamic approach for swollen polymers proposed by Frenkel<sup>16</sup> and Flory and Rehner<sup>17</sup> was considered. The average molecular weight between crosslinks  $M_{c,\text{swelling}}$  was determined using Equation (4), based on the phantom network model<sup>18</sup>:

$$M_{c,\text{swelling}}, \text{kg mol}^{-1} = \frac{-\rho_{\text{polymer}} V_{m,\text{toluene}} \left(\phi_p^{\frac{1}{3}}\right) f - 2}{\ln(1 - \phi_p) + \phi_p + \chi \phi_p^2} \frac{f - 2}{f}, \quad (4)$$

where  $\rho_{\text{polymer}}$  is the polymer density ( $0.00113 \text{ kg cm}^{-3}$ ),  $V_{m,\text{toluene}}$  is the molar volume of toluene ( $106.29 \text{ cm}^3 \text{ mol}^{-1}$ ),  $\chi$  is the Flory-Huggins polymer-solvent interaction parameter,  $\phi_p$  is the volumetric polymer fraction in the swollen gel, and  $f$  is the crosslink functionality, taken as 4,<sup>19</sup> since the polymer under study has a high molecular weight, thus is composed of long macromolecules. The factor that relates the fraction of elastically active material  $w_{\text{el}}$ , is present at the original equation proposed by Schlögl et al.<sup>18</sup> was omitted due to experimental limitations of performing solid-state low-field MQ <sup>1</sup>H NMR in the swollen state. The volumetric fraction of polymer in the swollen gel was calculated as described by Equation (5), where considerations regarding the filler mass fraction  $\Phi_{\text{filler}}$  (determined by thermogravimetric analysis, TGA) were taken, since it does not swell in the presence of toluene:

$$\phi_p = \frac{\frac{m_{\text{dry}} - \Phi_{\text{filler}} m_{\text{dry}}}{\rho_{\text{polymer}}}}{\frac{m_{\text{dry}} - \Phi_{\text{filler}} m_{\text{dry}}}{\rho_{\text{polymer}}} + \frac{m_{\text{swollen}} - m_{\text{dry}}}{\rho_{\text{toluene}}}}. \quad (5)$$

In the above equation,  $m_{\text{dry}}$  was used instead of  $m_{\text{initial}}$  as a correction for the mass loss due to toluene solubility of chemicals ( $\text{Sol}_{\text{tol}}$ ) that are incorporated into the rubber network, like peroxide decomposition by-products and low molecular weight macromolecules. The sample density was considered as constant after swelling, based on the findings by Valentín et al.<sup>15</sup> Assumptions or corrections regarding the network degradation due to swelling were not considered here, since peroxide-cured rubbers, unlike sulfur-cured organic rubber compounds, are considered to not significantly degrade during the experiment.<sup>15</sup> The Flory-Huggins polymer-solvent interaction parameter  $\chi$  for the pair silicone-toluene was taken

as a function of  $\phi_p$ , as reported by Kuwahara et al.<sup>20</sup> according to Equation (6):

$$\chi = 0.445 + 0.297\phi_p. \quad (6)$$

Several studies in the literature consider the Flory-Huggins polymer-solvent interaction parameter  $\chi$  as constant. However, since  $\chi(\phi_p)$  was available for PDMS, it was applied here. In the case where this function is not yet disclosed, a fixed and determined value should be used. Since all swelling experiments were conducted at the same temperature ( $23^\circ\text{C}$ ), the dependency of  $\chi$  on temperature was neglected.

### 2.4.1 | Practical aspects for the swelling experiments

In order to obtain reliable and statistically valid results for the equilibrium swelling experiments, it is advisable that a strict and fixed protocol is followed for every sample that is tested. In the present investigation, equilibrium swelling experiments were carried out according to the *modus operandi* developed by the authors.

Regarding sampling, it is advisable that all samples have roughly the same weight, which should be at least two orders of magnitude higher than the sensitivity of the applied scale. Besides, the samples should have similar surface areas (or shape), in order to avoid differences regarding the solvent contact area. It is advisable that the samples do not touch each other, neither the bottom, nor the side walls of the glass flask where the experiment is conducted, also to avoid differences in solvent contact area.

As regards to the flask where the experiment is carried out, ideally it should be made of glass. If organic elastomers are the case of study, the flasks must be kept away from direct light, aiming to avoid chemical degradation. In the case of silicones, this is not an issue, since poly(dimethylsiloxane)s are composed of fully saturated molecules. During the whole experiment, the flask must be sealed, protected from light, and in stable and controlled temperature and humidity.

For the solvent, a compatible liquid should be chosen (toluene) considering not only safety and availability, but also the ease of working with. Toluene has a vapor pressure ( $20^\circ\text{C}$ ) of 29 hPa, while water's is around 17 hPa, for example. A widely used solvent for swelling experiments is chloroform ( $\text{CHCl}_3$ ), which has a much higher vapor pressure: 210 hPa. This means that it is harder to handle chloroform than toluene, since the former evaporates faster, causing mass loss when conducting the swelling experiment. A high vapor pressure is more critical when

the swelling is over, since the sample must be slightly blotted and weighed, avoiding excessive solvent loss to the ambient air. Thus, it is advisable to look for compatible, safe, available, and slightly volatile solvents to avoid errors.

About weighing the swollen samples, attention must be paid when operating the scale. Since an organic solvent is present, safety measures must be taken to avoid inhaling toxic vapors. Besides, it is advisable to work with a second glass flask inside the scale, enabling to put the swollen sample inside the mentioned flask, close it, and finally weigh it. This procedure avoids excessive solvent evaporation, limiting it to the necessary to reach equilibrium with the air inside the flask.

If a drying stage is necessary, attention must be paid to the thermal degradation of the swollen sample. It is advisable to evaporate the solvent at low temperatures (20°C below the solvent boiling temperature) and with the aid of vacuum, if available. Drying at the fume hood at room temperature can be done, but a second drying stage in higher temperature is necessary. The drying process is finished when the sample reaches constant weight within the sensitivity of the scale.

After drying, it is advisable to compare the dry mass and the initial mass of the same sample. This procedure allows one to observe mass losses during swelling. If mass loss is detected and it is at least higher than the mass standard deviation among the samples, a correction for the applied equations (calculation of the polymer fraction in the swollen gel) is necessary. The same applies to filled samples, where the filler content must be discounted from the measured masses, since filler particles hardly swell in organic solvents.

## 2.5 | Proton low-field solid-state NMR spectroscopy

Static low-field time-domain multi-quantum  $^1\text{H}$  NMR spectroscopy experiments were performed at room temperature on a benchtop spectrometer (Minispec mq20, Bruker, Billerica, MA, USA), operating at the Larmor resonance frequency of 20 MHz ( $B_0 = 0.47$  T) with a 90° pulse length and receiver deadtime of 1.6 s and 15  $\mu\text{s}$ , respectively. Two millimeter thick/8 mm diameter disks were punched out of both the non-crosslinked (pure PDMS gum) and the crosslinked PDMS plates and stacked (until a maximum height of 10 mm) inside a glass tube, which was then placed into the spectrometer. The experiment was performed without replication, due to the stability of the method and of the device.

$^1\text{H}$  NMR data were measured and analyzed according to previously published procedures.<sup>21,22</sup> Relevant

parameters were taken from the data fitting procedure, like the so-called residual dipolar coupling constant  $D_{\text{res}}$ , reflecting the constraint density (crosslink points and entanglements); the logarithmic standard deviation of the probability distribution of residual couplings in the sample, or width parameter  $\sigma_{\text{ln}}$ ; and the fractions of isotropically mobile moieties, such as network defects (characterized by a long effective relaxation time), here identified as tail 1 (relaxation time = 15–25 ms) and tail 2 (relaxation time >60 ms).

The average molecular weight between crosslinks  $M_{c,\text{NMR}}$  was evaluated using Equation (7), based on a fixed-junction model and explicit spin dynamics simulations, considering the phantom network model as the theoretical basis,<sup>19,23</sup> 1266 Hz as the calibration value  $D_{\text{ref}}$  for poly(dimethylsiloxane), and the crosslink functionality  $f$  as 4:

$$M_{c,\text{NMR}}, \text{ kg mol}^{-1} = \frac{1266 f - 2}{\frac{D_{\text{res}}}{2\pi} f}. \quad (7)$$

## 2.6 | Positron annihilation lifetime spectroscopy

Positron annihilation lifetime spectroscopy (PALS) measurements were performed using disk-shaped samples (20 mm diameter, 2 mm thickness), where all positrons entering them were annihilated.  $^{22}\text{Na}$  was used as the positron source, embedded between two Kapton (polyimide) foils, and placed inside a copper cup containing the sample. This whole set was arranged in contact with a liquid nitrogen cryostat (DN 1714 Oxford Instruments, Abingdon, Oxfordshire, England), capable of providing a 0.5 K stability on temperature within the  $-135$  to  $40^\circ\text{C}$  range. Measurements were performed at a pressure lower than  $10^{-5}$  mbar. The collection of the positron spectra was accomplished using a fast-fast timing spectrometer (340 ps resolution), and each spectrum contained at least  $2 \times 10^6$  counts. The spectrometer was composed of two plastic scintillators (Pilot U, 1.5" diameter, 1" height) connected to photomultipliers (Philips XP2020, Philips, Amsterdam, Netherlands). Analysis of the spectra was performed by means of a dedicated program for such purpose (LT program<sup>24</sup>) with a proper correction for the positron annihilation occurring at each of the Kapton supports (thickness of 7  $\mu\text{m}$ ). The experiment was performed without replication, due to the stability of the method and of the device.

PALS allows the indirect measurement of how large the cavities within a certain polymer network are. In the

present study, the samples at different temperatures were shot with positrons. Interaction of thermalized positrons with matter via diffusion may cause the formation of an unstable bound system, positronium (Ps), which is the same size as hydrogen, but about 2000 times lighter.<sup>25</sup> This atomic system is pushed into the open volumes of the material, where the electron density is lower, due to the exchange repulsion between the Ps electron and the external electrons. Ground state Ps in vacuum exists in two sub-levels, para-Ps (antiparallel spins, lifetime 125 ps) and ortho-Ps, o-Ps (parallel spins, lifetime 142 ns). Annihilation occurs in two (para-Ps) and three photons (o-Ps), respectively.<sup>26</sup>

Ps is the atomic system usually employed and its annihilation is detected in PALS experiments. Indeed, Ps in open spaces of polymers, such as free volume holes in the amorphous regions and defects in the crystalline domains, may annihilate, in addition to its own electron, also with an external electron in relative singlet state. This “pickoff” process allows annihilation in two photons and this channel greatly reduces o-Ps lifetime with respect to vacuum. Ps lifetime is correlated to the size of the cavity where annihilation occurs. Such a relationship between o-Ps lifetime and the size of holes in polymer networks is the central point of PALS analyses.

## 2.7 | Mechanical and physical properties characterization

Uniaxial tensile tests were performed according to DIN (Deutsche Institut für Normung) 53504<sup>27</sup> with a universal testing machine (Zwick Roell, Ulm, Germany) using a 10 kN load cell at a constant crosshead speed of 200 mm min<sup>-1</sup> at room temperature. Smooth dumbbell specimens were cut from 2 mm crosslinked plates, leading to specimens with 2 mm thickness and 4 mm width, that were clamped at a distance of 25 mm. For each formulation, the average and standard deviation values of the moduli at 100% (M100) and 300% (M300) elongations of five samples were reported.

Dynamic mechanical analysis of the crosslinked PDMS samples was performed in a DMA device (MCR 702e MultiDrive, Anton Paar GmbH, Graz, Austria) in tensile mode. An identical thermal program was applied to all samples, starting from room temperature and cooling down (2 K.min<sup>-1</sup>) to -150°C. Subsequently, a 5 min isotherm was held, before finally heating up (2 K min<sup>-1</sup>) the sample to 50°C. A dynamic strain of 0.07% was applied with a frequency of 1 Hz. The glass transition temperature  $T_g$  was taken as the tan  $\delta$  apex between -150 and -100°C. The sample 1.5 phr was analyzed in triplicate to determine the overall variation of the

experiment, which for the glass transition temperature determination was less than 1%.

Hardness determination was conducted at room temperature according to DIN ISO (International Organization for Standardization) 48-4.<sup>28</sup> Six millimeter thick crosslinked plates were tested in a digital Shore A durometer (Hardness Tester HT 3000 MonTech Rubber Testing Solutions GmbH, Buchen, Germany) and the hardness was measured in triplicate.

## 3 | RESULTS

This section is divided into three major subsections. The first, comprehending Section 3.1, discusses the effect that the crosslinking has on the crystallization and melting of the silicone samples. The second, including Section 3.2, reports on the molecular weight between crosslinks for different DCP concentrations, along with a comparison between the swelling and the static low-field time-domain multi-quantum <sup>1</sup>H NMR spectroscopy experiments. Finally, mechanical properties are discussed in the third Section 3.3, where the effects of different DCP concentrations on the mechanical properties are assessed, as well as considerations regarding free volume are made.

### 3.1 | Crystallization and melting behavior

Non-crosslinked and crosslinked samples were analyzed by DSC to obtain information regarding the DCP concentration effect on the melting of PDMS crystallites and on

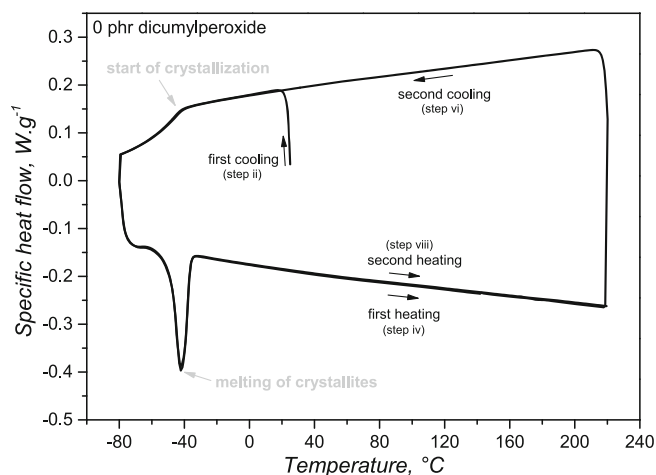


FIGURE 1 DSC thermogram of the non-crosslinked PDMS sample without DCP, with indications for the main thermal events and the sequence of heating/cooling ramps. Exo up.

the heat release related to the exothermic reactions of DCP decomposition and of crosslink formation. Figure 1 shows the thermogram for a pure solid PDMS rubber, without DCP. According to observation, a broad signal appears at  $-40^{\circ}\text{C}$  during cooling, due to the start of PDMS crystallization, which is completed during the isotherm of stage iii (described in Section 2.3). PDMS crystallization occurs due to the high flexibility of the siloxane macromolecules, which are able to organize into lamellae structures. These structures grow from small nuclei, which are formed in the bulk of the polymer network. Considering that the sample under investigation has sufficiently high molecular weight to promote a high density of chain entanglements,<sup>29,30</sup> it is fair to assume that nucleation on the melt rubbery state occurs far from a chain entanglement, and that the growth lamellae has a fine structure, due to the highly entangled state of high molecular weight and highly flexible PDMS.<sup>31</sup> The presence of a mineral filler dispersed into the rubber matrix and its influence on the nucleation phase of temperature-induced crystallization is still unclear. Even though it is reported that filler particles affect polymer chain conformations and local reptation,<sup>32</sup> the effect they have on nucleation is argued to be negative by some authors,<sup>33</sup> since fillers create a region with hindered mobility where the nucleation and crystallite growth are slowed down; neutral by others,<sup>34</sup> claiming that fillers extensively affect only the crosslinking reaction, not the crystallization; and positive by some,<sup>35</sup> that suggest fillers favor the formation of nuclei via polymer chain adsorption, interaction, or

even confinement of macromolecules inside a filler network.

On the first heating (stage 4), an endothermic signal is present, indicating the melting of crystallites that were formed during cooling and during the isotherm at  $-80^{\circ}\text{C}$ . Melting demands energy to occur, since the organized lamellae structure is only destroyed when the macromolecules have enough thermal energy to move and assume a higher entropic state, characterizing an endothermic event at the DSC. The melting peak temperature is within the typical range for silicones,<sup>36,37</sup> around  $-40^{\circ}\text{C}$ , and its shape reflects the crystallites' morphology in terms of size distribution, that is, the sharp peak for the pure solid PDMS rubber indicates a narrow size distribution for the crystals. No exothermic peak is observed at higher temperature, which is evident due to the absence of DCP and due to the high thermal stability of poly(dimethylsiloxane)s, that only start degrading above  $300^{\circ}\text{C}$ .<sup>38,39</sup>

The first (step 4) and second (step 8) DSC heating ramps for the DCP/PDMS systems are shown in Figure 2, with the region of crystallite's melting shown in Figure 2a. Analysis of the melting endothermic signal at approximately  $-40^{\circ}\text{C}$  grants the evaluation on how the DCP content (thus, the crosslinking extent) affects PDMS crystallization. The melting enthalpy, represented by the area of the melting peak, decreases after crosslinking reaction for all samples, regardless of the peroxide content, indicating that the sample crystallinity also decreases due to the linkage of adjacent PDMS macromolecules (crosslinks). All crosslinked systems

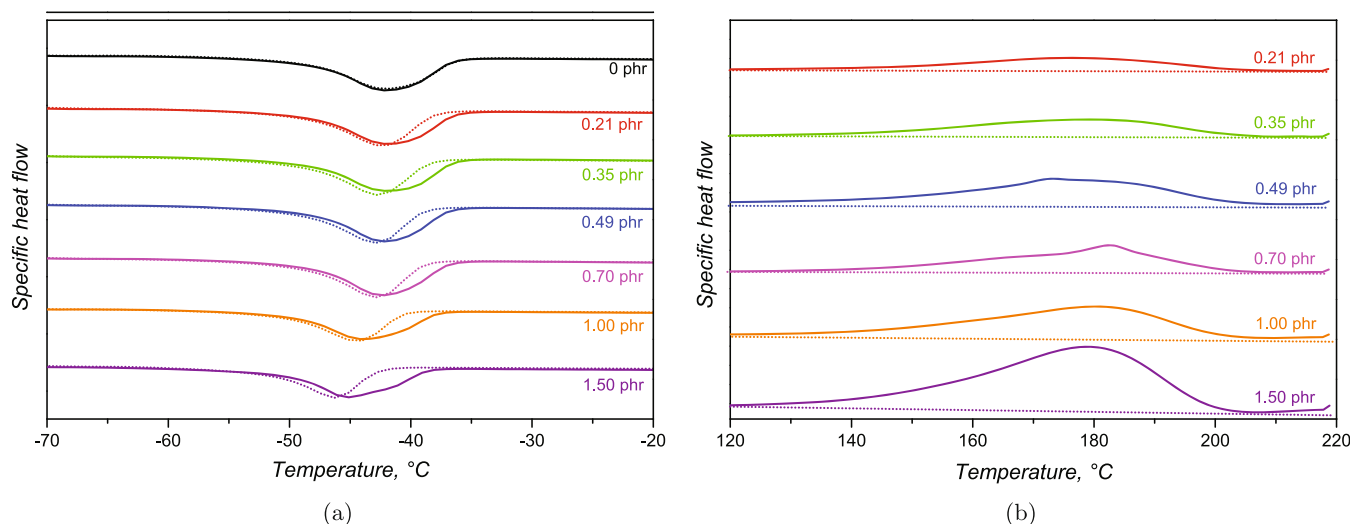


**FIGURE 2** DSC thermograms for the PDMS/DCP systems with varied dicumylperoxide concentrations, highlighting the thermal events including the endothermic melting (a) and the exothermic crosslinking (b). The full lines indicate the first heating (stage 5, non-crosslinked sample) and the dotted lines indicate the second heating (stage 8, crosslinked sample). Exo up. [Color figure can be viewed at [wileyonlinelibrary.com](http://wileyonlinelibrary.com)]

underwent a decrease in crystallinity that varied from 0% to 14%, when compared to their analogous non-crosslinked pair, from which the associated enthalpy values can be seen at Figure 3a. The decrease in PDMS' crystallinity after crosslinking was also reported by Roland and Aronson,<sup>40</sup> where a justification for this finding was given: the tetrafunctional junctions (crosslinks) constrain 8–9 chain units from being incorporated into the crystal phase.<sup>40</sup> The decrease of melting enthalpy related to the non-crosslinked samples (first heating) among the samples 0–0.70 phr and the samples with higher DCP concentrations (1 and 1.5 phr) is justified by batch differences between these two groups of samples, as discussed in Section 2.1.

Another parameter that enables the evaluation on how crosslink formation affects crystallinity is the melting peak temperature. Differently from the enthalpy, the melting peak temperature is related to the stability and to the size of crystallites. A decrease of the melting temperature is noticeable after crosslinking (Figure 3b), meaning that the imposed chemical constraints result in less stable and possibly smaller crystallites. This melting point depletion was also reported by Roland and Aronson<sup>40</sup> and by Sui et al.<sup>41</sup> the latter who investigated gamma-irradiated PDMS.

It is important to mention the effects imposed by physical entanglements in the nucleation (precedent phase to crystallite growth) and by chemical crosslinks in the crystallite, or lamellae, growth. It is commonly accepted that entanglements counteract crystallization,<sup>31,42–45</sup> but also crosslink junctions are said to inhibit crystallite growth. Even though the present study and others demonstrated

the previously mentioned behavior, Dollase et al.<sup>46</sup> observed the opposite trend for low molecular weight poly(siloxane)s. Still, in the same publication, the authors suggest that the distance between crosslinks determines the thickness of the crystallite's lamellae, also preventing crystallite thickening/growth, which is what probably occurred to the samples analyzed in the present investigation. It was not possible, however, to observe a specific trend for the melting enthalpy depletion and the DCP concentration. This is possibly justified by the low concentration range and the spatially heterogeneous nature of peroxidic crosslinking,<sup>47</sup> which is characterized by locally crosslinked clusters.

Nevertheless, all PDMS/DCP systems, even in the crosslinked state, were able to crystallize. This fact suggests that the molecular weight between crosslinks is large enough (chain segment between two crosslink knots is long enough) to enable crystallization. This finding is corroborated by the MQ <sup>1</sup>H NMR and swelling experiments, discussed further in this publication, which confirmed a molecular weight between crosslinks in the order of magnitude of the critical molecular weight between entanglements  $M_e$  for poly(dimethylsiloxane). The assessment of PDMS' crystalline phase allows the detection of molecular changes due to crossli, however, a correlation with mechanical properties should be made with cautiousness, since most silicone products are applied in temperatures highly above the melting temperature. That means that during service, mechanical loads are transferred to a completely amorphous network, which lacks reinforcement from the crystalline phase, but possesses only entanglements and crosslink points as network features.

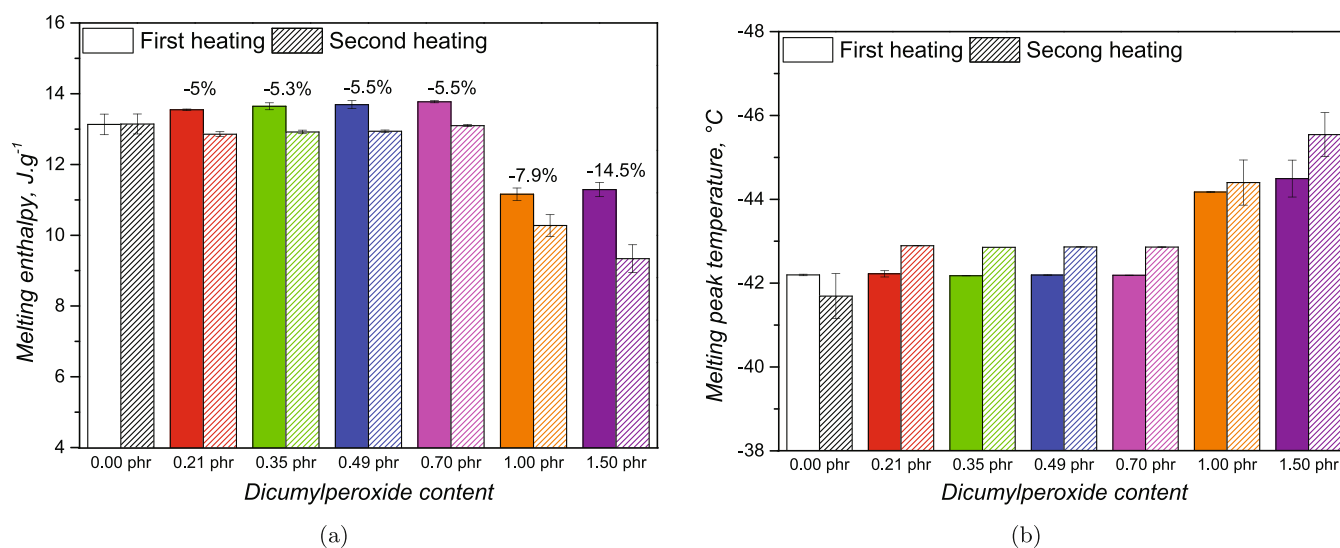


**FIGURE 3** Melting enthalpy (a) and melting peak temperature (b) for the non-crosslinked (first heating) and crosslinked (second heating) PDMS/DCS systems with varied DCP contents. For the melting enthalpy, it is noted above the respective bar the enthalpy depletion after curing. [Color figure can be viewed at [wileyonlinelibrary.com](http://wileyonlinelibrary.com)]



Analysis of the exothermic crosslinking signal (highlighted at Figure 2b) shows that the signal intensity rises as the DCP concentration increases, meaning that the enthalpy related to this thermal event also increases. The increase in enthalpy due to the higher DCP content is plausible: a higher number of DCP molecules also increases the energy released by both the peroxide decomposition reaction (which is exothermic<sup>48,49</sup>) and the crosslinking reaction. This justification was also used and understood as plausible in this group's publication<sup>8</sup> that dealt with the crosslinking kinetics of these DCP/PDMS systems. It is important to point out that the signal detected by DSC over the range 100–200°C is related to two first subsequent, and later concomitant, reactions: the DCP's thermal decomposition (homolytic cleavage of the O—O bond) and the formation of C—C covalent bonds (crosslink junction). These reactions are said to be first subsequent to each other because it is necessary that first one DCP molecule decomposes, in order to generate radicals to start the crosslinking reaction. After radical generation, the crosslinking reaction proceeds concomitantly to the formation of more radicals. The exothermic signal finally vanishes after all radicals have been consumed, either via formation of crosslink points, or due to termination, via hydrogen transfer or disproportionation, for example.

Differential scanning calorimetry is not able to distinguish the heat that is released from the peroxide decomposition and the heat from the formation of crosslink points. Even though the enthalpy must be proportional to both reactions, it is known and already reported in a previous publication of this group<sup>8</sup> that the DCP-based curing, in terms of radical formation, does not guarantee full efficiency of radical hydrogen abstraction, since termination and side reactions may occur. However, it is possible to state that the majority of DCP molecules were (statistically) decomposed, since no exothermic peak is observed at the second heating. This fact leads to the

point where studying a peroxide-based crosslinking reaction only by DSC is insufficient, since the peroxide decomposition kinetics may overcome, or at least conceal, the rubber crosslinking. Rheology methods, which are also widely used for such purpose, rely on the increase in modulus, which is a clear reflection of a network formation, without ambiguities or concurrent effects.

### 3.2 | Molecular weight between crosslinks evaluation

Determining the molecular weight between crosslink points is a task that can be accomplished using different methodologies.<sup>50</sup> Swelling tests in a suitable solvent are rather simple methods to determine the crosslinking state of a polymer specimen and the results of these tests for the silicone rubber compounds with varied DCP concentrations are shown in Table 1. The effect of the DCP concentration on the swelling degree SD is evident, since crosslinking adjacent silicone macromolecules prevents the polymer network from swelling, due to the lower interaction of solvent molecules with polymer chains. The fraction of toluene-soluble matter is kept almost constant with the DCP concentration, but representing less than 4% of the specimen mass. This fact justifies the use of  $m_{\text{dry}}$  instead of  $m_{\text{initial}}$  in Equation (5) to account for this mass loss, which possibly comprehends soluble silicone oligomers and crosslinking by-products. The molecular weight between crosslinks is calculated using Equation (4), which is based on the phantom network model, first introduced by James and Guth<sup>51</sup> and further developed by Graessley.<sup>52</sup> This model assumes that the elastically effective polymer macromolecules can cross each other freely without compromising the network morphology, meaning that the forces that arise during the swelling test are merely transmitted to the crosslink

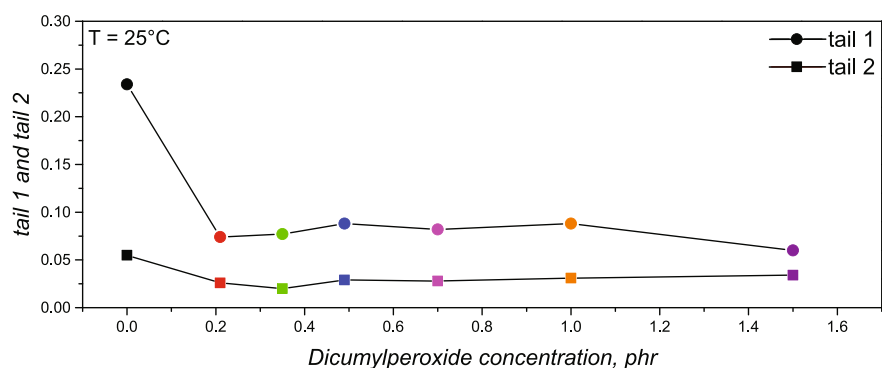
**TABLE 1** Equilibrium swelling results and solid-state low-field multi-quantum <sup>1</sup>H NMR determined parameters for silicone rubber compounds with varied dicumylperoxide concentrations.

Sample (phr)	SD (%)	Sol <sub>toluene</sub> (%)	$M_{c,\text{swelling}}$ (kg mol <sup>-1</sup> )	$\sigma_{\text{ln}}$ (-)	tail 1 (-)	tail 2 (-)	$D_{\text{res}}/2\pi$ (Hz)	$M_{c,\text{NMR}}$ (kg mol <sup>-1</sup> )
0	n/a	n/a	n/a	0.632	0.234	0.055	34.9	18.14
0.21	183.0 ± 0.4	3.64 ± 0.03	8.36	0.352	0.074	0.026	89.9	7.04
0.35	180.9 ± 0.1	3.64 ± 0.01	8.20	0.290	0.077	0.020	92.0	6.88
0.49	177.0 ± 0.2	3.50 ± 0.04	7.90	0.299	0.088	0.029	97.4	6.50
0.70	176.7 ± 0.3	3.50 ± 0.01	7.97	0.288	0.082	0.028	102.7	6.16
1.00	171.0 ± 0.8	3.78 ± 0.06	7.44	0.264	0.088	0.031	106.0	5.97
1.50	170.0 ± 0.1	3.74 ± 0.02	7.37	0.297	0.060	0.024	107.3	5.90

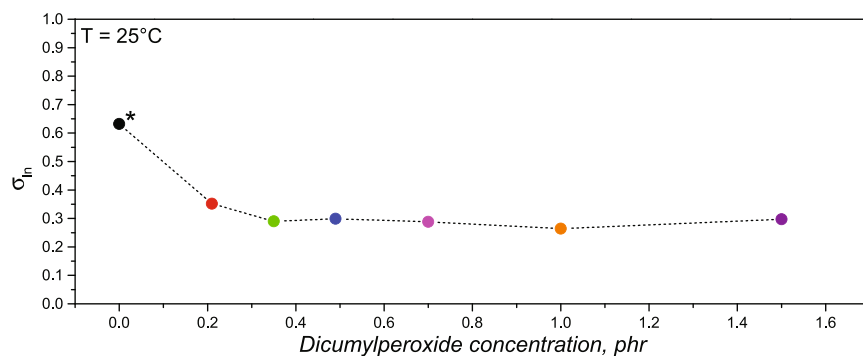
joints to which the chains are linked.<sup>53</sup> From the values reported in Table 1, one can realize that the molecular weight between crosslinks  $M_{c,swelling}$  decreases with the DCP concentration, that is, the crosslink density increases as more radicals are formed. However, even though there is an evident decrease of the molecular weight between crosslinks, this increase is not as high as expected for the DCP concentration range that was employed. In fact, from 0.21 to 1.50 phr (increase of more than 600%), the  $M_{c,swelling}$  decreased by only 10%. Theoretically calculating the number of mers (chain segments with molecular weight of  $74 \text{ g mol}^{-1}$ ) of silicone that are excluded from the chain in-between crosslinking when the peroxide concentration increases from 0.21 to 1.50 phr, this number is limited to only 13 mers approximately. A threshold for the crosslinking extent seems to exist for this crosslinking system, as the molecular weight between entanglements approaches the value of  $8 \text{ kg mol}^{-1}$ .

Solid-state multi-quantum  $^1\text{H}$  NMR experiments normally shed light into the understanding of how the molecular dynamics occurs into polymeric networks. The values for the parameters that are obtained after sample testing are also reported in Table 1, along with a graphic representation in Figure 4. The parameter  $\sigma_{ln}$ , or width parameter, contains information about the homogeneity of the polymer network and usually  $\sigma_{ln} > 0.4$  denotes inhomogeneous crosslinked networks. All crosslinked samples (DCP concentration  $> 0$  phr) present a narrow

$D_{res}$  distribution ( $\sigma_{ln} < 0.4$ ), meaning that they possess rather homogeneous networks in terms of the spatial distribution of crosslinks and entanglements. Higher values for  $\sigma_{ln}$  would occur only when the spatial distribution of constraints is inhomogeneous on the lengthscale beyond 5 nm, that is, exceeding one or a few network chain sizes.<sup>54</sup> In the present case, chain packing (due to entanglement and crosslinking) and connectivity effects (local force balances) “homogenize” the NMR response. The non-crosslinked sample 0 phr presents  $\sigma_{ln} > 0.4$  (marked with a \* sign at Figure 4b), which does not mean it is a non-homogeneous network, but that it is a linear polymer undergoing reptation motion, which is indeed the case of poly(dimethylsiloxane). Reptation motion is the movement of a polymer chain confined within a tube-like region, usually driven by random thermal agitation.<sup>55</sup> This theoretical approach<sup>56,57</sup> takes into consideration that the macromolecules cannot move perpendicular to their own contour, but only along it. The tail 1 and tail 2 values (Figure 4a) for the crosslinked samples show that they have around 8% of non-elastic but high molecular weight defects, such as dangling chains, for example; and around 3% of low molecular weight defects, like outer chain ends. These values related to defects are in accordance with the high molecular weight and the molecular weight distribution of the silicone rubber under investigation: less than 2% of the macromolecules have lower than  $100 \text{ kg mol}^{-1}$  before crosslinking. In



(a)



(b)

FIGURE 4 MQ  $^1\text{H}$  NMR parameters variation with the dicumylperoxide concentration. Tail 1 and tail 2 (a), and  $\sigma_{ln}$ , or  $D_{res}$  distribution length, where the non-crosslinked sample is marked with a \* signal (b). [Color figure can be viewed at [wileyonlinelibrary.com](http://wileyonlinelibrary.com)]

addition, the polymer's high molecular weight induces a minor response of the chain ends, whose concentration decreases as the molecular weight increases during polymerization. It is important to point out that the three parameters seem to be around a threshold value, without significant changes when the DCP concentration increases.

Values for the residual dipolar coupling constant  $D_{\text{res}}/2\pi$  are also reported in Table 1. A slight increase is observed among the crosslinked samples as the DCP concentration increases, pointing to a saturation or threshold of the crosslink density. The same behavior was previously reported<sup>8</sup> for the maximum detected torque values during rheometry measurements using a rubber process analyzer, which reflects the cure state of the elastomer. As stated in Equation (7), the molecular weight between crosslinks can be estimated, which directly shows the tendency to an equilibrium state of cure.

Regarding the non-crosslinked sample 0 phr, the residual dipolar coupling constant amounted to 34.9 Hz (representing an apparent molecular weight between entanglements of  $18.14 \text{ kg mol}^{-1}$ , value that is higher than the true  $M_e$ , due to reptation), which is lower than the usually reported 90 Hz value for poly(dimethylsiloxane), that was measured at a lower temperature where the experimental timescale corresponds to the entanglement time  $\tau_e$ .<sup>22</sup> This discrepancy is explained by the high molecular weight of the silicone rubber under investigation within the scope of the present paper ( $M_w = 660 \text{ kg mol}^{-1}$ ), its linear chain morphology, and the reptation motion associated to this precursor, as compared to the PDMS studied by Chávez and Saalwächter.<sup>22</sup>

For visualization, a schematic of the progressive change in the PDMS/DCP network is shown at Figure 5. At the non-crosslinked state, the network has only entanglements, and the macromolecules are able to move

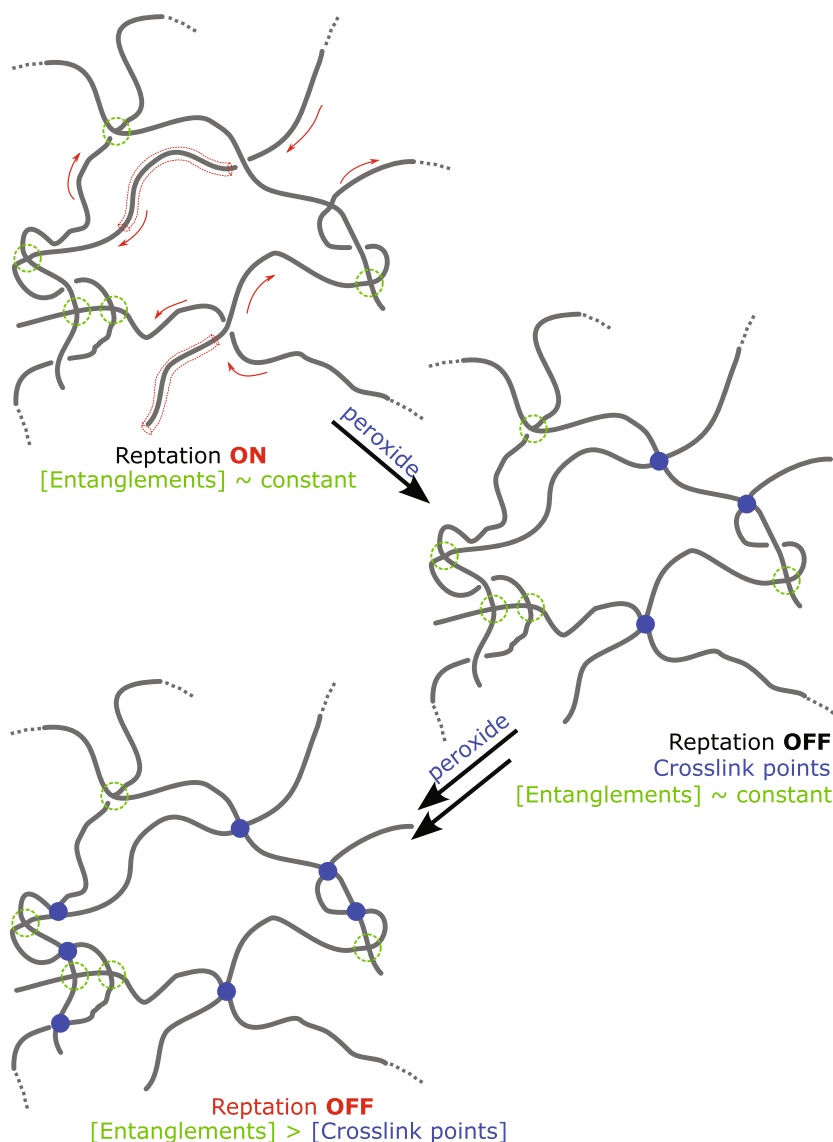


**FIGURE 5** Schematic representation of the progressive curing of a highly entangled network. The reptation tube is represented by a red dashed line, while the red arrows indicate the reptation motion itself. Entanglements are indicated by green dashed circles, and crosslink points by blue solid circles. The concentration of green dashed circles and blue solid circles as represented by this figure are only representative, since the concentration of entanglements overcomes the concentration of crosslink points. [Color figure can be viewed at [wileyonlinelibrary.com](http://wileyonlinelibrary.com)]

confined along the reptation tube. After DCP addition, reptation is frozen, and crosslink points are incorporated to the network. At the final stage, that is, higher concentration of DCP and complete crosslinking, both entanglements and crosslink points co-exist at the network, dictating all properties of such network.

Equilibrium swelling tests and solid-state low-field multi-quantum  $^1\text{H}$  NMR experiments provide insights into the crosslink state of elastomer and usually their findings agree with each other. The comparison between the constant  $D_{\text{res}}/2\pi$  and the crosslink density  $1/M_{c,\text{swelling}}$  as determined by the swelling tests, is presented in Figure 6a. The methods result in a similar behavior, which is widely reported in the literature.<sup>58,59</sup> By fitting  $D_{\text{res}}$  to a linear function, it is expected that the intercept, that is, the theoretical point where the DCP concentration

is zero, reflects the contribution of a free-of-crosslinks sample (only entangled) to  $D_{\text{res}}$ .<sup>18</sup> In the present case, the extrapolated value is close to 85 Hz, in good agreement with the entanglement-related value mentioned above. The relationship between the crosslink densities  $1/M_c$  as determined by swelling and by low-field  $^1\text{H}$ -NMR is also shown in Figure 6b, where both quantities are plotted for the studied DCP concentrations. This correlation is roughly linear as expected but has a slope exceeding unity due to uncertainties in calculating  $1/M_c$ . With regards to  $1/M_{c,\text{swelling}}$ , variations arise from the Flory-Huggins polymer-solvent interaction parameter  $\chi$ , which is reported in the literature (for the pair silicone-toluene) by several authors.<sup>20,60–62</sup> For the present study,  $\chi(\phi_p)$  was chosen as described by Kuwahara et al.<sup>20</sup> since it was determined for solutions of linear PDMS without adding any model uncertainty, as stressed by Chassé et al. in the correction of their article.<sup>19</sup> Concerning  $1/M_{c,\text{NMR}}$ , calculation issues are related to Equation (7), which is model-dependent. The most relevant issue is likely the omission of the defect-related correction (consideration of the fraction of elastically active material  $\omega_{\text{el}}$ ), which must be based upon NMR experiments in the swollen state, being beyond the scope of the present work.

Worth mentioning is the fact that the measured  $D_{\text{res}}/2\pi = 34.9$  Hz for the 0 phr sample does not automatically point to the molecular weight between entanglements contribution of a crosslinked sample, as one would mistakenly suggest by analogy with the molecular weight between crosslinks. Schlögl et al.<sup>18</sup> reported that the  $D_{\text{res}}$  for non-crosslinked linear precursor can be directly assumed as the entanglement contribution of the same elastomer, if the analysis is carried out at the same temperature. However, for crosslinked systems this is ambiguous. This is due to the fact that the results for the non-crosslinked elastomer are strongly affected by temperature, while the  $D_{\text{res}}$  constant values for crosslinked polymeric networks are not. By assuming a constant entanglement density with the crosslinking state and the additivity of entangled and crosslinked chain densities, one can write:

$$D_{\text{res}} \sim \begin{aligned} &\text{crosslinking contribution} \\ &+ \text{entanglement contribution} \\ &= \frac{1}{M_{c,\text{NMR}}} + \frac{1}{M_e} \end{aligned} \quad (8)$$

Indeed, the case of  $D_{\text{res}}/2\pi = 34.9$  Hz does not represent solely the molecular weight between entanglements, but is a consequence of the polymer's finite molecular weight.

Considering the value of  $D_{\text{res}}/2\pi \approx 85$  Hz as the entanglement contribution and that the entanglement

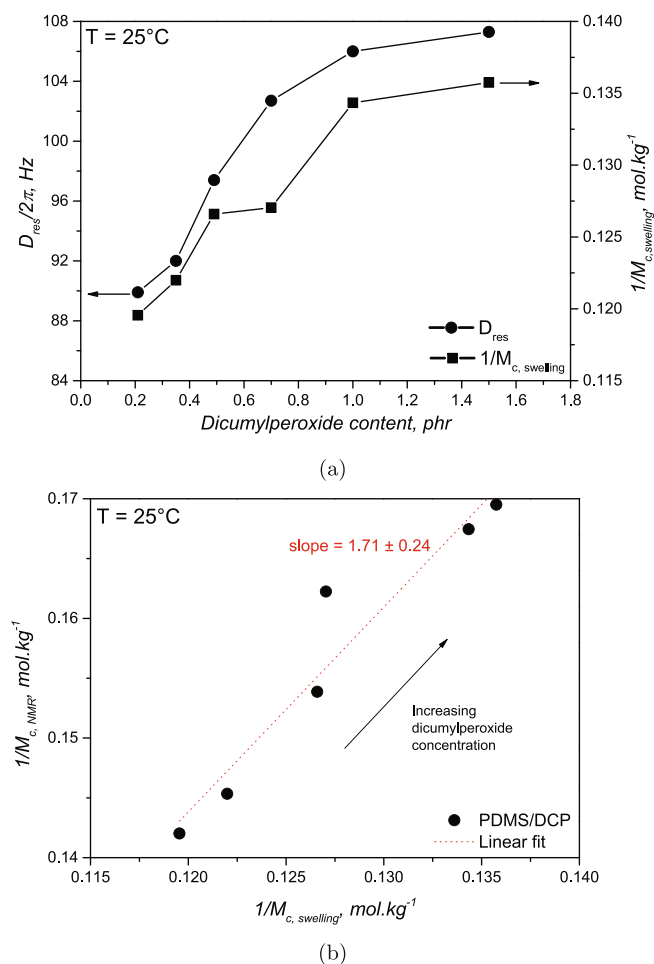


FIGURE 6 Comparison between the residual dipolar coupling constant  $D_{\text{res}}/2\pi$  and the crosslink density  $1/M_{c,\text{swelling}}$  as a function of the dicumylperoxide (DCP) concentration (a), and comparison between the crosslink densities  $1/M_{c,\text{swelling}}$  and  $1/M_{c,\text{NMR}}$  for increasing DCP concentration samples, at  $25^\circ\text{C}$  (b). The red dashed line represents the linear fitting, whose slope is shown. [Color figure can be viewed at [wileyonlinelibrary.com](http://wileyonlinelibrary.com)]

density does not change with the crosslink state, it is possible to state that the DCP-cured samples under investigation are dominated by entanglements, even after crosslinking. The very high molecular weight, highly above the critical molecular weight for entanglements for poly(dimethylsiloxane) ( $M_w$  of  $29 \text{ kg mol}^{-1}$ <sup>29</sup> or  $34.5 \text{ kg mol}^{-1}$ <sup>30</sup>), already induced an intensively entangled network even at the non-crosslinked state, reflected by the high viscosity of the solid silicone. Crosslinking this highly entangled network only slightly changes the molecular dynamics, but greatly enhances the elastic response of the elastomer, as will be discussed in the next sections. Counter-intuitively, the increasing DCP concentration did not cause major changes on the molecular weight between crosslinks most likely due to the thermodynamics and the chemical mechanism that controls the respective curing reaction, as already noted previously.<sup>8</sup>

### 3.3 | Thermo-mechanical and mechanical properties

Dynamic mechanical analysis provides information regarding the thermo-mechanical properties of the PDMS/DCP

compounds, such as the extensional elastic/storage modulus  $E'$  and the extensional plastic/loss modulus  $E''$ , as well as the relationship between them:  $\tan \delta$ , or extensional loss factor. Both moduli are plotted in Figure 7a, where glass transition, characterized by its temperature  $T_g$ , can be assigned as the  $E'$  drop between  $-125$  and  $-100^\circ\text{C}$ , or the apex of  $E''$  at the same temperature range. This range for the glass transition is typical and is already reported elsewhere.<sup>63</sup> The glass transition temperature of poly(dimethylsiloxane) is the lowest of all synthetic elastomers, specifically due to its molecular structure. Poly(dimethylsiloxane) macromolecules possesses flexible backbones, with long chain bonds ( $106 \text{ kJ mol}^{-1}$  and  $1.64 \text{ \AA}$ , compared to  $85 \text{ kJ mol}^{-1}$  and  $1.53 \text{ \AA}$  for C—C bond<sup>1</sup>), and wide bond angles (Si—O—Si bond angle of  $143^\circ$ , compared to  $109.5^\circ$  of the usual tetrahedron bond angles<sup>2</sup>), allowing easier side-group rotation. In this sense, the molecular motion at low temperatures is still present, due to the cooperative crankshaft motion of the silicon and oxygen atoms, as described by Schatzki.<sup>64</sup> In the present case, the crankshaft movement of 8 alternating silicon/oxygen atoms provides enough flexibility for the macromolecule to only freeze below  $-125^\circ\text{C}$ , characterizing the very low  $T_g$  of silicone.

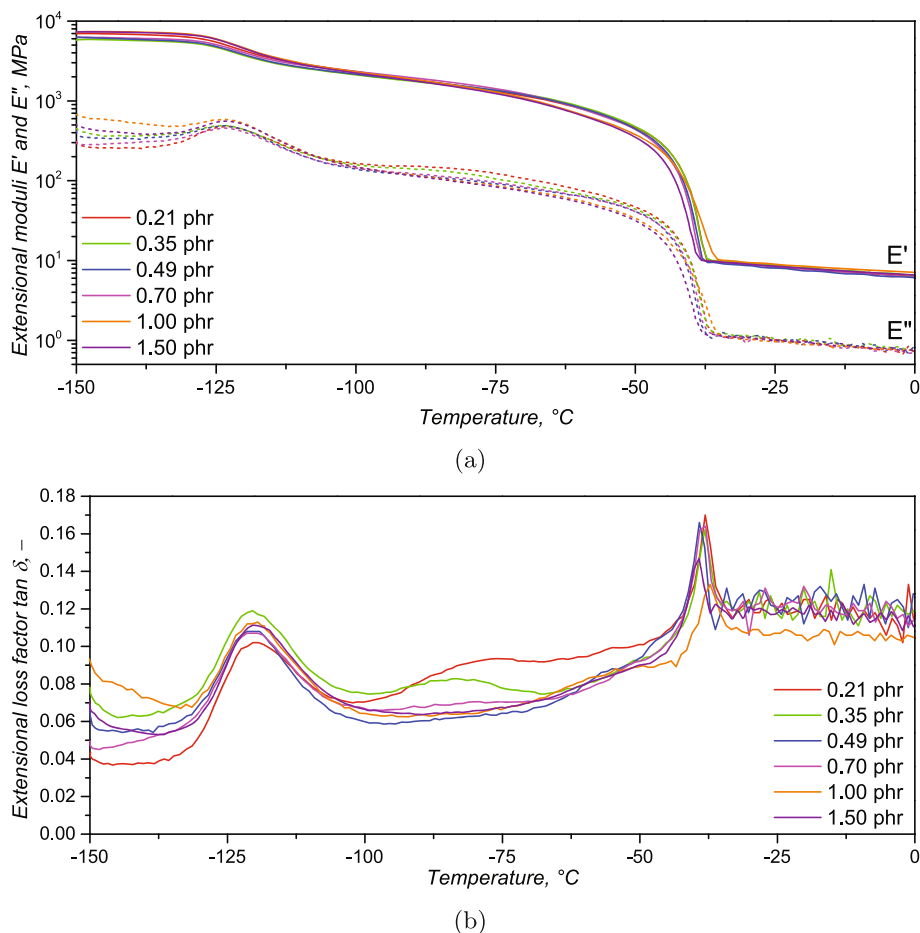


FIGURE 7 Dynamic mechanical behavior of the varied DCP/PDMS systems. Extensional storage and loss moduli (a), and extensional loss factor  $\tan \delta$  (b). [Color figure can be viewed at [wileyonlinelibrary.com](https://onlinelibrary.wiley.com)]

At temperatures above the glass transition, the samples soften, but still present a rather high elastic modulus  $E'$  (higher than  $10^3$  MPa) due to the self-reinforcing effect of the crystallites formed during cooling, and their action as physical crosslink points. All silicone samples underwent crystallization during the slow cooling ( $-2$  K  $\text{min}^{-1}$ ), in a temperature range obviously above the glass transition temperature, where the molecules still had enough flexibility and thermal energy to move, organize into lamellae, nucleate and, ultimately, crystallize. When  $-50^\circ\text{C}$  is reached, melting of the crystalline phase occurs, in agreement with the DSC thermograms reported in Figure 2a. Melting of crystallites causes the moduli to abruptly drop, due to the lack of self-reinforcement. Finally, after melting, the samples reached the actual rubbery plateau, whose values are characteristic for room temperature and filled silicone samples.

For a further analysis of the glass transition region, the loss factor  $\tan \delta$  is shown in Figure 7b. The glass transition temperature  $T_g$  was assigned as the apex of the  $\tan \delta$  signal between  $-125$  and  $-100^\circ\text{C}$  and reported in Table 2. No significant difference and no trend were observed for the temperature where the samples passed from brittle to soft, being at around  $-120^\circ\text{C}$ . This suggests that the molecular movement related to the glass transition is not hindered neither by the crosslinking points, nor by the entanglements, which dominate the samples' network as shown before. Indeed, considering the 8-atom crankshaft movement and the molecular weight between crosslinks as reported in Table 1, no

movement suppression happened with the increase of DCP concentration: comparing the 0.21 phr and the 1.50 phr samples, a total of approximately 16 mers are excluded from the in-between crosslinked segments. These 16 mers have 32 alternating silicon/oxygen atoms, which are enough for the cooperative movement that ultimately leads to the glass transition. Another conclusion can be taken from the aforementioned facts: a constant glass transition temperature regardless of the state of cure may also reflect on a constant free volume hole size, which is proven by the PALS experiments.

Figure 8 shows the variation of o-Ps lifetime  $\tau_3$  with temperature for the non-crosslinked (0 phr) and one crosslinked sample (0.70 phr). Within the temperature range  $-160$  to  $50^\circ\text{C}$ , the free volume hole size (correlated to  $\tau_3$ ) changes according to different temperature zones. Below the glass transition temperature ( $T < -130^\circ\text{C}$ ),  $\tau_3$  slightly increases with temperature, which reflects the limited chain motion that hinders the free volume hole expansion.<sup>65</sup> When the glass transition temperature is reached, the  $\tau_3$  variation changes, represented by a change in the slope. At the glass transition region and above, the free volume hole size increases at a higher rate, due to the higher molecular motion, mainly thermally driven.

Another difference in the slope is observed at the melting temperature region, already reported in the literature and assigned to the PDMS crystallites' melting.<sup>66</sup> After melting and until room temperature is reached, considering the typical standard deviation for PALS

Sample (phr)	M100 (MPa)	M300 (MPa)	Hardness (–)	$T_g$ ( $^\circ\text{C}$ )
0.21	$0.95 \pm 0.01$	$2.51 \pm 0.04$	$48.0 \pm 0.1$	$-120.43$
0.35	$0.96 \pm 0.01$	$2.65 \pm 0.08$	$48.3 \pm 0.5$	$-119.86$
0.49	$0.99 \pm 0.02$	$2.79 \pm 0.09$	$48.7 \pm 0.5$	$-120.41$
0.70	$1.02 \pm 0.01$	$3.01 \pm 0.17$	$49.3 \pm 0.5$	$-120.23$
1.00	$1.17 \pm 0.02$	$3.68 \pm 0.06$	$49.8 \pm 0.4$	$-119.51$
1.50	$1.11 \pm 0.06$	$3.68 \pm 0.26$	$50.2 \pm 0.3$	$-120.29$

TABLE 2 Tensile moduli at 100 (M100) and 300% (M300) of deformation and Shore A hardness values for the various crosslinked samples at  $25^\circ\text{C}$ , along with the correspondent glass transition temperature  $T_g$ .

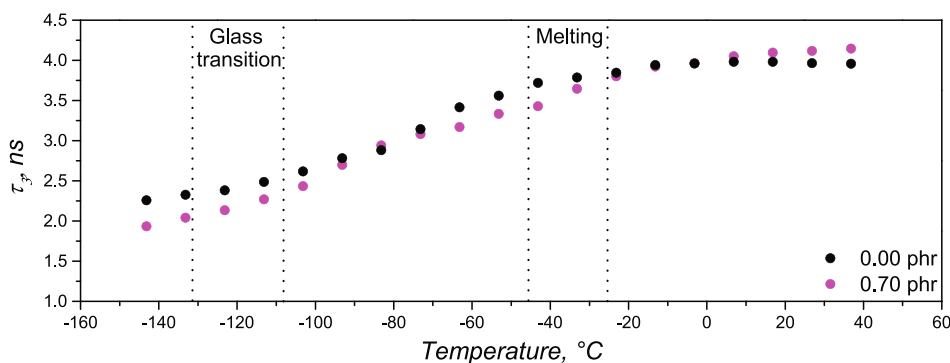


FIGURE 8 o-positronium (o-Ps) lifetime variation with temperature for the 0 phr and the 0.70 phr DCP/PDMS samples. [Color figure can be viewed at [wileyonlinelibrary.com](http://wileyonlinelibrary.com)]

experiments,<sup>65,66</sup> both non-crosslinked and crosslinked samples presented the same  $\tau_3$  value. A constant  $\tau_3$  value for increasing crosslinked PDMS samples was also reported by Sui et al.<sup>41</sup> This fact leads to the inference that the free volume hole size does not change after crosslinking, evidently proven by the DMA experiments. In this sense, it is still expected that the free volume hole size, in the present case, is mainly controlled by molecular packing, and not by the crosslink points or the entanglements.

The main mechanical properties as function of the DCP concentration are listed in Table 2, along with the temperature associated to the glass transition. For both moduli, an increase is observed as the DCP concentration rises, mainly due to the denser crosslinked network that is formed after curing. The denser the networks, the more effective is the load transfer from one molecule to the next, joined by the crosslink point, and ultimately causing the tensile strength to increase. This increase was already expected, since this group has already reported<sup>8</sup> that the maximum torque values measured by a moving die rheometer during curing also experience an increment. However, as previously observed for the maximum torque and for the crosslink density assessments,<sup>8</sup> the moduli also reach a threshold. For all these findings, a constant increase with the DCP concentration is not present, revealing again a limitation of crosslinking.

Regarding the Shore A hardness values, a slight increase is observed as the DCP concentration rises, reaching the typical value of 50 Shore A for this silicone rubber grade. Kruželák et al.<sup>12</sup> and Verheyen et al.<sup>13</sup> reported the exact same trend for hardness when studying DCP-crosslinked rubbers. However, none of the aforementioned authors suggests a reason why the increment in the DCP concentration does not proportionally reflect an increase in these properties. As a matter of comparison, an increase of more than 600% on the DCP concentration (0.21 phr compared to 1.50 phr), resulted in a 15% increase for M100, 46% increase for M300, and 5% for the hardness. Considering that the hardness determination is a static measurement, the influence of the filler content is the main responsible for this property, with less contribution from the crosslink density. Besides, Shore A hardness assessment is a measurement method that mainly reflects the surface properties of an elastomer.

## 4 | CONCLUSIONS

This work reported a comprehensive description and discussion about the effects of DCP concentration on poly(dimethylsiloxane) rubber networks. The investigation

was justified and based on macromolecular reasonings, considering how the crosslink points affect thermal behavior, mechanical properties, and molecular dynamics.

Crosslinking PDMS with DCP caused a decrease in the potential of crystallization and a destabilization of the formed lamellae. Besides, it resulted in rather homogeneous networks, when entanglements and crosslink points are considered. The effect of DCP concentration on the crosslink density was evident, as proven by swelling and NMR experiments. However, all samples showed a similar network dynamics, mainly dominated by entanglements.

By analyzing all characterization methods using a holistic approach, it is possible to realize the counter-intuitive effect of the DCP concentration on the PDMS' network morphology. As it would be expected, the increase in the DCP concentration would cause a proportional change in several properties. However, in the case of DCP and the present polymer (solid silicone rubber with the determined vinyl content), the studied DCP concentration range caused a response regarding the investigated properties that reached a plateau. This is understood to be caused by the dominance of entanglements over crosslink points and the characteristic crosslinking mechanism that governs curing.

As not usually trivial or reported, an in-depth study of DCP-cured solid silicone rubber, widely used in the elastomer industry, was carried out. The findings of this work help to comprehend the importance of dosing crosslinking agents when rubber formulation is executed, aiming to avoid over-dosing. In the present investigation, a direct correlation between crosslinker concentration and performance was made, justified by molecular reasoning, showing that an increase of concentration not always leads to a proportional influence on a given property. In addition, this report also contributes to the overall understanding of elastomer networks' properties and how their micro and macro-responses behave when the tridimensional polymer network changes, as, for example, via crosslinking.

## AUTHOR CONTRIBUTIONS

**M. Azevedo:** Conceptualization (lead); data curation (lead); formal analysis (lead); investigation (lead); methodology (lead); writing – original draft (lead); writing – review and editing (lead). **A. -M. Monks:** Data curation (supporting); formal analysis (supporting); investigation (supporting); writing – review and editing (supporting). **R. C. Kerschbaumer:** Conceptualization (supporting); formal analysis (supporting); funding acquisition (lead); methodology (supporting); project administration (lead); supervision (lead); writing – review and editing (supporting). **S. Schlögl:** Formal analysis

(supporting); writing – review and editing (supporting). **K. Saalwächter:** Data curation (supporting); formal analysis (supporting); writing – review and editing (supporting). **M. Walluch:** Data curation (supporting); formal analysis (supporting); writing – review and editing (supporting). **G. Consolati:** Data curation (supporting); formal analysis (supporting); writing – review and editing (supporting). **C. Holzer:** Funding acquisition (supporting); project administration (supporting); supervision (supporting); writing – review and editing (supporting).

## ACKNOWLEDGMENTS

The research work of this paper was performed at the Polymer Competence Center Leoben GmbH (PCCL, Austria) within the framework of the COMET-program of the Federal Ministry for Climate Action, Environment, Energy, Mobility, Innovation and Technology and the Federal Ministry for Digital and Economic Affairs, with contributions from the Montanuniversitaet Leoben (Department of Polymer Engineering and Science, Polymer Processing and Materials Science and Testing of Polymers), Martin-Luther Universitaet Halle-Wittenberg (Institut für Physik - NMR), Anton Paar GmbH, and Politecnico di Milano (Department of Aerospace Science and Technology). The authors kindly acknowledge Bernard Lechner and Gerald Meier for experimental support. PCCL is funded by the Austrian Government and the State Governments of Styria, Lower Austria, and Upper Austria.

## FUNDING INFORMATION

The research work presented at this publication was part of the COMET project “Innovative material characterization methods for reactive systems” number 1072920 (ReaSys project) and accomplished within the framework of the COMET-program of the Austrian Federal Ministry for Climate Action, Environment, Energy, Mobility, Innovation and Technology and the Federal Ministry for Digital and Economic Affairs.


## CONFLICT OF INTEREST STATEMENT

M. Azevedo, A. -M. Monks, R. C. Kerschbaumer, and S. Schlögl are employed by Polymer Competence Center Leoben GmbH, and M. Walluch is employed by Anton Paar GmbH. The companies had no role in the design of the study, in the collection, analyses, or interpretation of data, in the writing of the manuscript, and in the decision to publish the results.

## DATA AVAILABILITY STATEMENT

All data presented in this publication are available under request to the corresponding author, assuming a formal approval of the involved companies and co-authors.

## ORCID

M. Azevedo  <https://orcid.org/0000-0001-7730-8642>  
 R. C. Kerschbaumer  <https://orcid.org/0000-0002-8847-4264>  
 S. Schlögl  <https://orcid.org/0000-0002-2840-9700>  
 K. Saalwächter  <https://orcid.org/0000-0002-6246-4770>  
 G. Consolati  <https://orcid.org/0000-0003-3614-245X>  
 C. Holzer  <https://orcid.org/0000-0001-5149-7895>

## REFERENCES

- [1] S. Shit, P. Shah, *Natl. Acad. Sci. Lett.* **2013**, *36*, 355.
- [2] J. Calderón, D. López, E. Pérez, J. Montesinos, *Polym. Bull.* **2020**, *77*, 2749.
- [3] J. Fink, *Liquid Silicone Rubber: Chemistry, Materials, and Processing*, John Wiley & Sons, Hoboken, NJ **2019**.
- [4] T. Köhler, A. Gutacker, E. Mejía, *Org. Chem. Front.* **2020**, *7*, 4108.
- [5] K. Mojsiewicz-Pienkowska, M. Jamrógiewicz, K. Szymkowska, D. Krenczkowska, *Front. Pharmacol.* **2016**, *7*, 132.
- [6] A. Rahimi, A. Mashak, *Plastics* **2013**, *42*, 223.
- [7] R. Ghunem, Y. Hadjadj, H. Parks, *Energies* **2021**, *14*, 3655.
- [8] M. Azevedo, A.-M. Monks, R.-C. Kerschbaumer, S. Schlögl, C. Holzer, *Polymer* **2022**, *14*, 4404.
- [9] D. Akbarian, H. Hamed, B. Damirchi, D. Yilmaz, K. Penrod, W. Woodward, J. Moore, M. Lanagan, A. van Duin, *Polymer* **2019**, *183*, 121901.
- [10] T. Chatterjee, S. Wiessner, K. Naskar, G. Heinrich, *Polym. Eng. Sci.* **2017**, *57*, 1073.
- [11] J. Heiner, B. Stenberg, M. Persson, *Polym. Test.* **2003**, *22*, 253.
- [12] J. Kruželák, S. Hakošová, A. Kvasničáková, I. Hudec, *KGK Kautschuk Gummi Kunststoff* **2020**, *73*, 36.
- [13] F. Verheyen, R.-U. Giesen, H.-P. Heim, *Int. Polym. Process.* **2017**, *32*, 337.
- [14] S. Heinze, A. Echtermeyer, *Appl. Sci.* **2018**, *8*, 2227.
- [15] J. Valentín, J. Carretero-González, I. Mora-Barrantes, W. Chassé, K. Saalwächter, *Macromolecules* **2008**, *41*, 4717.
- [16] J. Frenkel, *Rubber Chem. Technol.* **1940**, *13*, 264.
- [17] P. Flory, J. Rehner, *Chem. Phys.* **1943**, *11*, 521.
- [18] S. Schlögl, M.-L. Trutschel, W. Chassé, G. Riess, K. Saalwächter, *Macromolecules* **2014**, *47*, 2759.
- [19] W. Chassé, M. Lang, J.-U. Sommer, K. Saalwächter, *Macromolecules* **2012**, *45*, 899.
- [20] N. Kuwahara, T. Okazawa, M. Kaneko, *J. Polym. Sci., Part C: Polym. Symp.* **1968**, *23*, 543.
- [21] L. Jakisch, M. Garaleh, M. Schäfer, A. Mordvinkin, K. Saalwächter, F. Böhme, *Macromol. Chem. Phys.* **2018**, *219*, 1700327.
- [22] W. Chassé, L. Valentín, G. Genesky, C. Cohen, K. Saalwächter, *Chem. Phys.* **2011**, *134*, 044907.
- [23] K. Saalwächter, B. Herrero, M. López-Manchado, *Macromolecules* **2005**, *38*, 9650.
- [24] J. Kansy, *Nucl. Instr. Methods Phys. Res. Sect. A* **1996**, *374*, 235.
- [25] G. Consolati, E. Mossini, D. Nichetti, F. Quasso, G. Viola, E. Yaynik, *Int. J. Mol. Sci.* **2021**, *22*, 1436.
- [26] F. Castelli, G. Consolati, G. Marlotti, *Nanomaterials* **2021**, *11*, 2350.
- [27] DIN. Testing of rubber - determination of tensile strength at break, tensile stress at yield, elongation at break and stress



- values in a tensile test, Standard DIN 53504:2017-03, Deutsches Institut für Normung. **2017**.
- [28] ISO 48-4:2018. Rubber, vulcanized or thermoplastic - determination of hardness - part 4: Indentation hardness by durometer method (shore hardness), Standard DIN/ISO 48-4, Deutsches Institut für Normung. **2018**.
- [29] G. Gordon, R. Schmidt, M. Quintero, N. Benton, T. Cosgrove, V. Krukonic, K. Williams, P. Wetmore, *Macromolecules* **2010**, *43*, 10132.
- [30] P. Dvornic, J. Jovanovic, M. Govedarica, *J. Appl. Polym. Sci.* **1993**, *49*, 1497.
- [31] R. Kurz, M. Schulz, F. Scheliga, Y. Men, A. Seidlitz, T. Thurn-Albrecht, K. Saalwächter, *Macromolecules* **2018**, *51*, 5831.
- [32] F. Nardelli, F. Martini, E. Carignani, E. Rossi, S. Borsacchi, M. Cettolin, A. Susanna, M. Arimondi, L. Giannini, M. Geppi, L. Calucci, *J. Phys. Chem. B* **2021**, *125*, 4546.
- [33] J. M. Chenal, L. Chazeau, Y. Bomal, C. Gauthier, *J. Polym. Sci., Part B: Polym. Phys.* **2007**, *45*, 955.
- [34] Y. Zhang, H. Zhou, *J. Appl. Polym. Sci.* **2020**, *137*, 49244.
- [35] J. Portal, C. Carrot, J.-C. Majeste, S. Cocard, V. Pelissier, I. Anselme-Bertrand, *Polym. Eng. Sci.* **2009**, *49*, 1544.
- [36] W. Wallau, C. Recknagel, G. Smales, *J. Appl. Polym. Sci.* **2021**, *138*, 50881.
- [37] A. Chien, R. Maxwell, S. DeTeresa, L. Thompson, R. Cohenour, B. Balazs, *J. Polym. Sci. Part B: Polym. Phys.* **2006**, *44*, 1898.
- [38] S. Shi, B. Lei, M. Li, X. Cui, X. Wang, X. Fan, S. Tang, J. Shen, *Prog. Org. Coat.* **2020**, *143*, 105609.
- [39] E. Camino, S. Lomakin, M. Lazzari, *Polymer* **2001**, *42*, 2395.
- [40] C. Roland, C. Aronson, *Polym. Bull.* **2000**, *45*, 439.
- [41] H. Sui, X. Lui, F. Zhong, X. Li, B. Wang, X. Ju, *Radiat. Eff.* **2014**, *169*, 628.
- [42] F. Peng, C. Nie, T.-Y. Xu, J. Sheng, W. Chen, W.-C. Yu, L.-B. Li, *Chinese J. Polym. Sci.* **2022**, *40*, 1640.
- [43] D.-C. Kong, M.-Y. Yang, X.-S. Zhang, Z.-C. Du, Q. Fu, J.-W. Gong, *Macromol. Mater. Eng.* **2021**, *306*, 2100536.
- [44] L. Xu, Z. Fan, *J. Chem. Phys.* **2002**, *117*, 6331.
- [45] K. Iwata, *Polymer* **2002**, *43*, 6609.
- [46] T. Dollase, H. Spiess, M. Gottlieb, R. Yerushalmi-Rozen, *Europhys. Lett.* **2002**, *60*, 390.
- [47] T. Saleesung, D. Reichert, K. Saalwächter, C. Sirisinha, *Polymer* **2015**, *56*, 309.
- [48] K.-T. Lu, Y.-C. Chu, R.-C. Chen, K.-H. Hu, *Process Saf. Environ. Prot.* **2010**, *88*, 356.
- [49] L.-C. Tsai, J.-W. Chen, H.-Y. Hou, S.-H. Liu, C.-M. Shu, *J. Therm. Anal. Calorim.* **2012**, *109*, 1303.
- [50] A. Blume, K. Kieseewetter, *KGK Kautschuk Gummi Kunststoffe* **2019**, *72*, 33.
- [51] H. James, E. Guth, *Chem. Phys.* **1943**, *11*, 455.
- [52] W. Graessley, *Macromolecules* **1975**, *5*, 186.
- [53] G. Hild, *Polymer* **1997**, *38*, 3279.
- [54] K. Saalwächter, J.-U. Sommer, *Macromol. Rapid Commun.* **2007**, *28*, 1455.
- [55] V. Boudara. Ph.D. thesis, University of Leeds. **2017**.
- [56] M. Doi, S. Edwards, *The Theory of Polymer Dynamics*, Oxford University Press, Oxford, UK **1988**.
- [57] P. de Gennes, *Chem. Phys.* **1971**, *55*, 572.
- [58] D. Fleischmann, S. Ayalur-Karunakaran, F. Arbeiter, R. Schaller, A. Holzner, W. Kern, S. Schlögl, *Polym. Test.* **2018**, *66*, 24.
- [59] D. Besghini, M. Mauri, R. Simonutti, *Appl. Sci.* **2019**, *1801*, 9.
- [60] F. Horkay, A.-M. Hecht, E. Geissler, *J. Polym. Sci. Part B: Polym. Phys.* **1995**, *33*, 1641.
- [61] S. Mallam, F. Horkay, A.-M. Hecht, A. Rennie, E. Geissler, *Macromolecules* **1991**, *24*, 543.
- [62] V. Soni, R. Stein, *Macromolecules* **1990**, *23*, 5257.
- [63] J. Zhao, N. Jiang, D. Zhang, B. He, X. Chen, *Polymer* **2020**, *12*, 1196.
- [64] T. Schatzki, *J. Polym. Sci.* **1962**, *57*, 337.
- [65] G. Consolati, G. Panzarasa, F. Quasso, *Polym. Test.* **2018**, *68*, 208.
- [66] G. Dlubek, U. De, J. Pionteck, N. Arutyunov, M. Edelman, R. Krause-Rehberg, *Macromol. Chem. Phys.* **2005**, *206*, 827.

**How to cite this article:** M. Azevedo, A.-M. Monks, R. C. Kerschbaumer, S. Schlögl, K. Saalwächter, M. Walluch, G. Consolati, C. Holzer, *J. Appl. Polym. Sci.* **2023**, *140*(31), e54111. <https://doi.org/10.1002/app.54111>